

Determining the Degree of Coulomb Coupling within the Inner Coma Dusty Plasma Environment of Comet 81P/Wild 2 with Stardust Data

Steven J. Pestana

California State Polytechnic University, Pomona

December 2015

1. Introduction

As emissaries of the frigid distant reaches of the Solar System, comets not only represent a physical separation from our home planet within the inner system but also a temporal one, as remnants of the system's building blocks in its earliest eons of formation. Thought to be composed of remnants of presolar nebular or interstellar cloud material, the dust within comets could shed light on the building blocks of the Solar System. Comets have been explored from afar first with the unaided human eye, then with Earth and space-based telescopes, and recently with variety of spacecraft flybys. These latest investigations have yielded information about the surface morphology (Brownlee et al, 2004), dust mineralogy (Fomenkova et al., 1992), gas composition, and the assortment of processes driving cometary activity.

The coma that surrounds a solid comet nucleus is made up of gas and dust components removed from the comet's surface through a variety of processes, most dramatically by the erupting jets of sublimating ices. These materials, in their new environment away from the nucleus, can undergo changes driven by the energy of the Sun. Photo-ionization creates a plasma environment within which comet dust particles reside, expanding outward from the inner coma.

The resulting dusty plasma environment within a comet's coma may exhibit characteristics that have been seen in other dusty plasma environments. One of these processes is the formation of Coulomb lattice structures. Upon being charged by the electron flux within a plasma, dust particles begin to self-organize into a lattice-like structure. Having been observed and studied within laboratory environments, these Coulomb lattice structures are thought to exist naturally in several dusty plasma environments including planetary ionospheres, planetary rings, and the coma of comets (Thomas et al., 1994).

In 2004 NASA's Stardust mission investigated comet dust within the inner coma of 81P/Wild 2 and returned samples of dust back to Earth. Using data from Stardust through NASA's Planetary Data System, this research project investigates the possibility that Coulomb

lattice structures could form within the coma of 81P/Wild 2, and analyzes if they were observed while Stardust explored the comet and its environs. The data from Stardust gives insight into the dust environment within cometary coma with an instrument suite designed to count and catalog particle collisions to supplement the spacecraft's particle sample collection tray which encapsulated dust particles to return to Earth. To complete the picture of the dusty plasma environment within the coma of 81P/Wild 2, a model of the comet's plasma environment is used to evaluate the dust-plasma interactions that could occur.

Understanding the space that surrounds comet nuclei will shed light on some of the dynamic processes that influence comet's near-nucleus, surface, and subsurface environments. Additionally, if the dusty plasma within the comet coma is home to Coulomb lattice structures, it would provide a natural setting for which to observe and study this unique plasma phenomena.

The results of this research project, however, do not reveal any obvious presence of Coulomb lattice formation within the regions surveyed by Stardust during its flyby of 81P/Wild 2. Based on the observed dust environment, it is found that the formation of such structures is heavily dependent on the volume density of dust particles at a spatial resolution too fine to be resolved by Stardust's instruments. The modeled plasma environment used does show a sufficient medium to support dust charging and lattice formation if provided with a dense enough cloud of dust particles. The European Space Agency's ongoing Rosetta mission, with its advanced suite of plasma physics instruments and extended mission, loitering low over the surface of comet 67P/Churyumov–Gerasimenko, will provide even better insight into this veiled environment of comets and dusty plasmas.

2. Background

2.1. Comets

The classification of comets into discrete families helps to identify the current distribution of the comet population by their orbital properties (Marsden, 2008). Recent processes that have affected comets might reflect their current orbital locations, or their current orbits, compositions and ongoing processes might reflect their regions of origin. Additionally, measuring and comparing the specific processes, compositions and dust to volatile ratios of comets could provide a classification system based on the inferred region of origin of the comets (Green, et al., 2004).

The body of a comet, the agglomerate dust and ice nucleus, becomes shrouded in a nebulous coma as volatile ices sublime. Observed morphologies and features within a comet's coma at distances close to the nucleus, such as conical jets or wider fans of sublimation products, suggest local changes in emission processes. Coma morphologies at distances further from the nucleus suggest interaction with the surrounding solar dominated environment (Farnham, 2009).

Solar energy warming volatiles trapped within a comet's assemblage near its surface causes pockets and regions of higher concentration of ices, notably water ice, to sublime and expand outward through surface material and away from the nucleus surface. Lofting dust particles high above the surface, these eruptions form expanding jets that can reach several nucleus radii from their former resting place below (Farnham, 2009). Micrometre-sized grains carried within these expanding gases can experience initial accelerations on the order of $10\text{-}100\text{ cm s}^{-2}$, varying inversely with particle mass. As these dust particles drift away from the nucleus, reaching distances of a kilometer in only a minute, they are slowed as gas drag takes its toll on their velocity with larger particles decelerating to less than 100 m s^{-1} . These jet formations, in the context of a spacecraft observing the processes of comet activity, are nearly instantaneous events at distances within the comet's inner coma (Sekania et al., 2004).

Peering from the inner Solar System, observations from Earth have yielded the discovery of a large number of comets, many of which can be classified as Jupiter-family comets (JFCs). The orbits of JFCs are dominated by the gravitational influence of Jupiter, though a more specific definition of this family of bodies is neither concrete nor undisputed (Marsden, 2008).

The Tisserand parameter can be used to roughly rein in a classification scheme for comets, specifically defining the requirements for being classified in a category such as JFCs. Derived from the orbital elements of a comet in question, the parameter describes the comet's relationship with the orbit of Jupiter (or any other large planet that might perturb a comet's orbit). This parameter shows robustness in that it can be used to identify objects such as comets both before and after close encounters with large planets like Jupiter that might alter the comet's orbit, since the value changes only slightly with such encounters (Marsden, 2008).

The equation for the Tisserand parameter, simplified for objects in relation to Jupiter is as follows:

$$T_j = a_j/a + (2 * \text{sqrt}(p/a_j) * \cos(i))$$

where the semi-latus rectum of the comet's orbit is p , and $p = q * (1+e)$. The comet's perihelion in AU is q , e is the comet's orbital eccentricity, and the semi-major axes of the comet's and Jupiter's orbits, in AU, are a and a_j , respectively. The inclination of the comet's orbit to the ecliptic in degrees is i (Marsden, 2008). Comets are generally classified as JFCs if they have a Tisserand parameter value of $2 < T_j < 3$ (+/- 0.1).

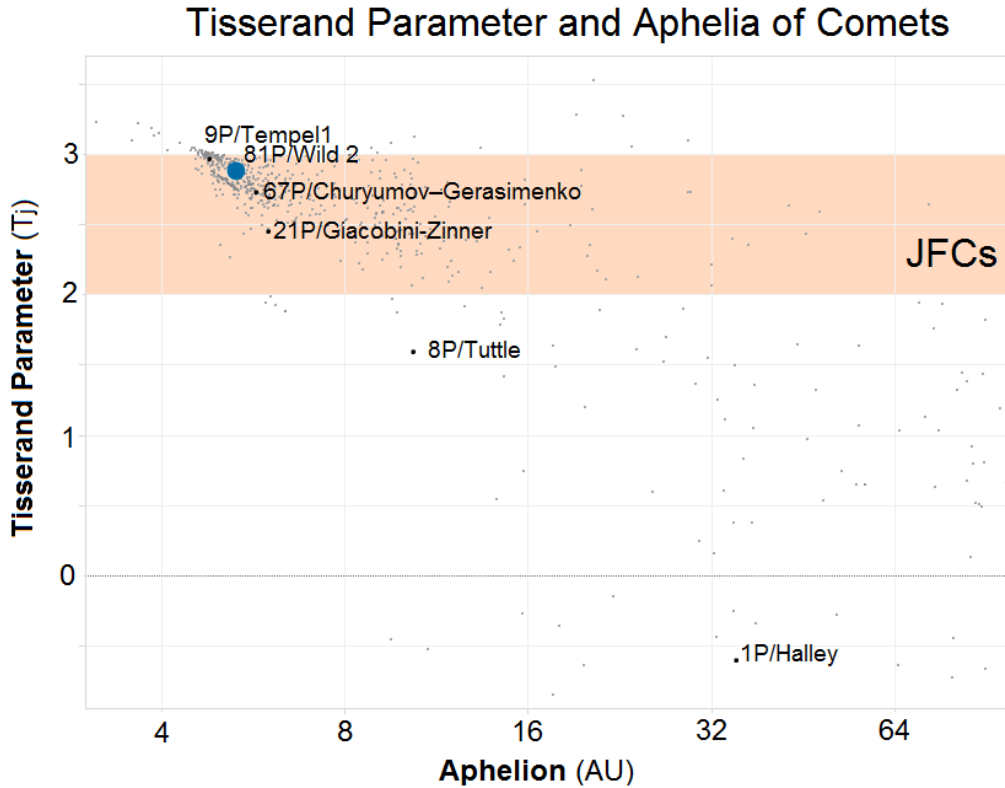


Figure 1. Tisserand Parameter, with respect to Jupiter (T_j), plotted against comet aphelion distance in AU. Some notable comets are labeled including 81P/Wild 2 (large blue circle). The Jupiter Family Comet (JFC) value range within $2 < T_j < 3$ is highlighted.

81P/Wild 2 belongs to this population of short period JFCs as classified by its orbital parameters and the derived Tisserand parameter. The orbit of 81P/Wild 2 brings it in towards the Sun with a perihelion of 1.49 AU and out towards the orbit of Jupiter with an aphelion of 5.2 AU over a period of 6.4 years. This region of the Solar System in which 81P/Wild 2 orbits, along with its associated Tisserand parameter, places it clearly within the JFC population.

Though not discovered until 1978, using its present-day orbit, it has been determined that before September of 1974 81P/Wild 2 had a much different orbit. This previous orbit is thought

to have taken the comet out to an aphelion of at least 19 AU, in the vicinity of, or beyond, the orbit of Uranus, and perihelion of 4.98 AU, towards Jupiter's orbit. This orbit would have had a period of approximately 57 years and an inclination between 13 and 20 degrees to the ecliptic. A close encounter with Jupiter in September of 1974 drastically altered the comet's orbit and established its present-day position as a JFC (Burchell, Kearsley 2009).

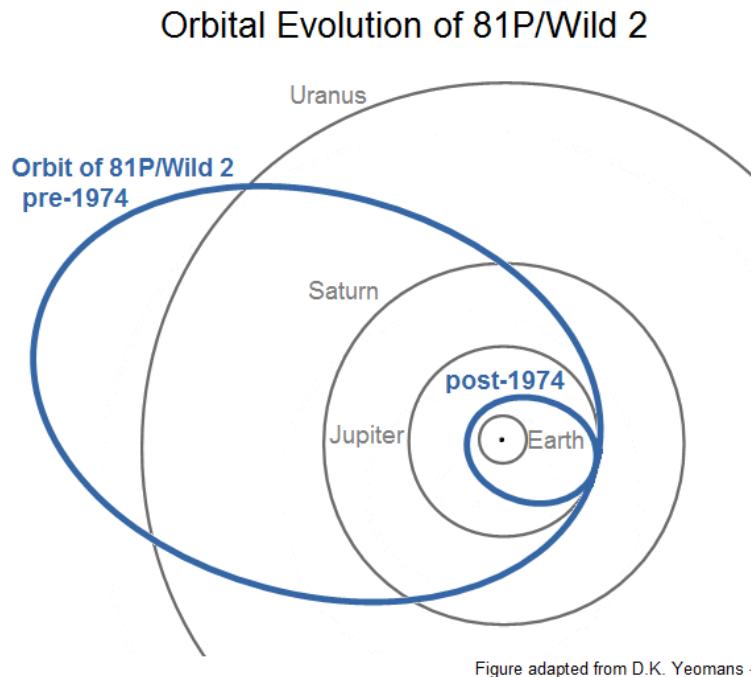


Figure 2. A close encounter with Jupiter in 1974 drastically altered the orbit of 81P/Wild 2, bringing it into the inner Solar System. This allowed Stardust to study relatively unaltered material from the outer Solar System, likely dating back to its formation.

At the time the Stardust spacecraft flew by 81P/Wild 2 in early 2004, the comet had only traversed its new Jupiter-family orbit four times, bringing it through perihelion only five times since its relocation from the outer Solar System. This provided an opportunity to study a comet that had been relatively undisturbed by strong insolation, representing a more pristine remnant of the early Solar System (Burchell, Kearsley 2009).

2.2. Stardust

Following the first generation of comet exploration missions that culminated in the flybys of comet 1P/Halley in 1986, Stardust was envisioned to reach a comet and collect samples of material within the coma and tail to be returned to Earth for study. Launched atop a Delta II

rocket in February of 1999 from Cape Canaveral Air Force Station in Florida, Stardust made its way to 81P/Wild 2 for nearly five years. On January 2nd, 2004, with a relative velocity of 6.1 km s⁻¹, Stardust performed its flyby of 81P/Wild 2, coming within 236.4 km of the comet's surface. The spacecraft made its approach from above the comet's orbital plane, passing through the coma region ahead of the comet's orbital path as 81P/Wild 2 passed by (Burchell, Kearsley 2009).

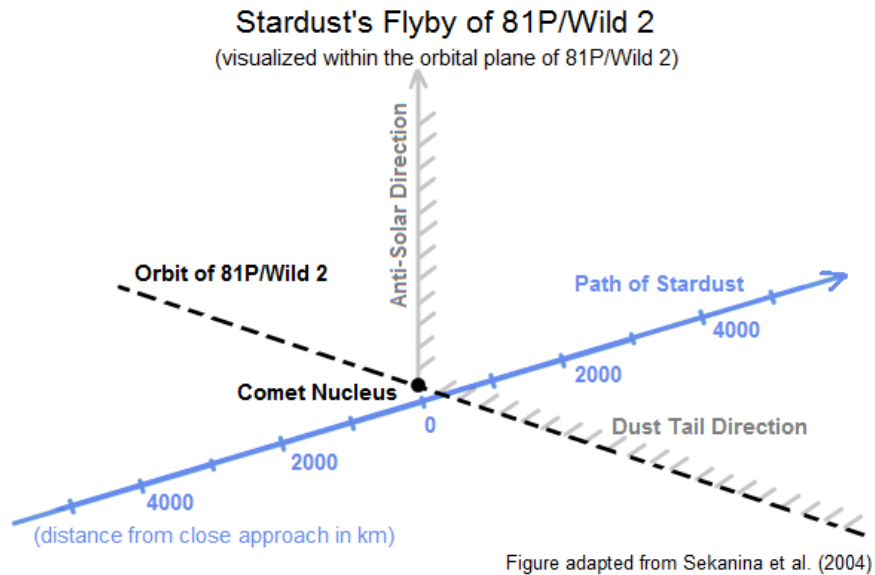


Figure 3. Visualized within the orbital plane of 81P/Wild 2, this figure shows the flyby geometry of Stardust and distance in kilometers with respect to the closest approach with the comet's nucleus. Also shown are the orbital path of the comet, and directions that gas and dust will trail behind or in the anti-Solar direction.

Passing through a comet's coma can reveal information about the spatial and mass distribution of dust surrounding the comet. This is the observation that Stardust's Dust Flux Monitor Instrument performed on January 2nd, 2004 as it flew past comet 81P/Wild 2 (Green et al., 2004). The Dust Flux Monitor Instrument (DFMI) gave Stardust the ability to collect particle flux and mass distribution data during its cruise phase and its flyby of 81P/Wild 2 through the comet's coma. Data from the DFMI contributed information to supplement the collection dust samples by the spacecraft, providing context to the environments from which the samples were gathered for their analysis back on Earth. For spacecraft engineering performance, health and analysis of anomalies that might have arisen, the DFMI could also have provided data to reveal issues regarding damaging particle collisions (Tuzzolino et al., 2003).

The DFMI was composed of two types of sensors and their associated electronics and mechanical support equipment: the PVDF sensors, from which the majority of data used in this project came from, and the Acoustic sensors.

The PVDF (polyvinylidene fluoride) sensor unit consisted of two circular thin-film sensors of permanently polarized material, one with a 28- μm thickness and 200 cm^2 of surface area, the other with a 6- μm thickness and 20 cm^2 of surface area. The PVDF sensors derive heritage from the Dust Counter and Mass Analyzer instrument (DUCMA) from the two Vega spacecraft that performed flybys of comet 1P/Halley in 1986 and the High Rate Detector (HRD) on-board the Cassini spacecraft in Saturnian orbit since 2004. Mounted on vibration absorbing pads to minimize spacecraft interference, high velocity dust impacts on the sensor's films produce cratering and holes, which in turn produce nanosecond current pulses with amplitudes corresponding to the impacting particle's mass. This sensor unit was mounted to the bumper panel that comprised the first layer of shielding on the front of the spacecraft bus (Tuzzolino et al., 2003).

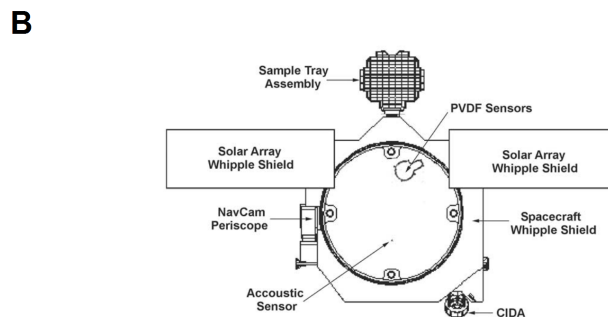
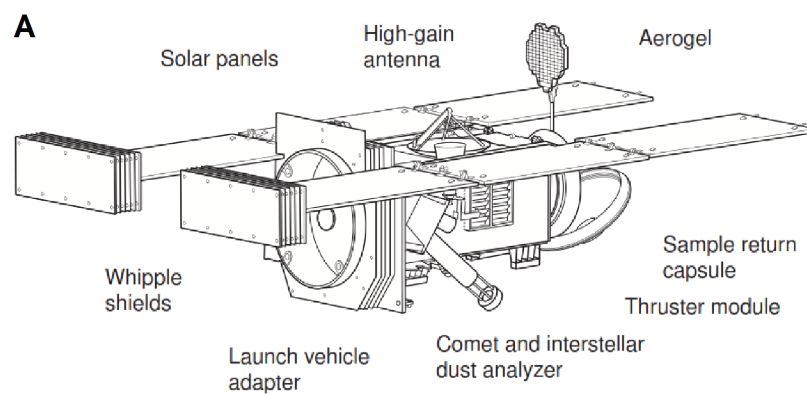


Figure 4. A) The Stardust spacecraft with some of its notable components labeled. The DFMI is housed within the launch vehicle adaptor region. **B)** Front view of Stardust showing the location and orientation of the DFMI PVDF sensors within the launch adaptor, sample collection tray and shielded solar arrays (Tuzzolino et al., 2003).

In order to measure higher mass particles that were expected to be encountered at a lower flux, two acoustic piezoelectric sensors were mounted to Stardust's front shielding. The A1 sensor was mounted to the rear of the front bumper panel, which had an effective surface area of about 0.7 m^2 . The A2 sensor was mounted to the front of an acoustic plate behind the front bumper panel with a surface area of 0.5 m^2 , capable of detecting particles large enough to penetrate the front bumper panel (Tuzzolino et al., 2003).

Stardust's sample collection and return tray consisted of 132 aerogel tiles, comprising a surface area of approximately 1039 cm^2 , and 287 aluminum foil sections covering 152 cm^2 . This tray, along with the embedded particles collected around 81P/Wild 2, descended to Earth's surface via parachute within the Sample Return Capsule (SRC) on January 15th, 2006. Following their return, the gel tiles and foils were examined using a variety of optical and electron microscopy to analyze dust particle impact distribution and trajectories (Westphal et al., 2008).

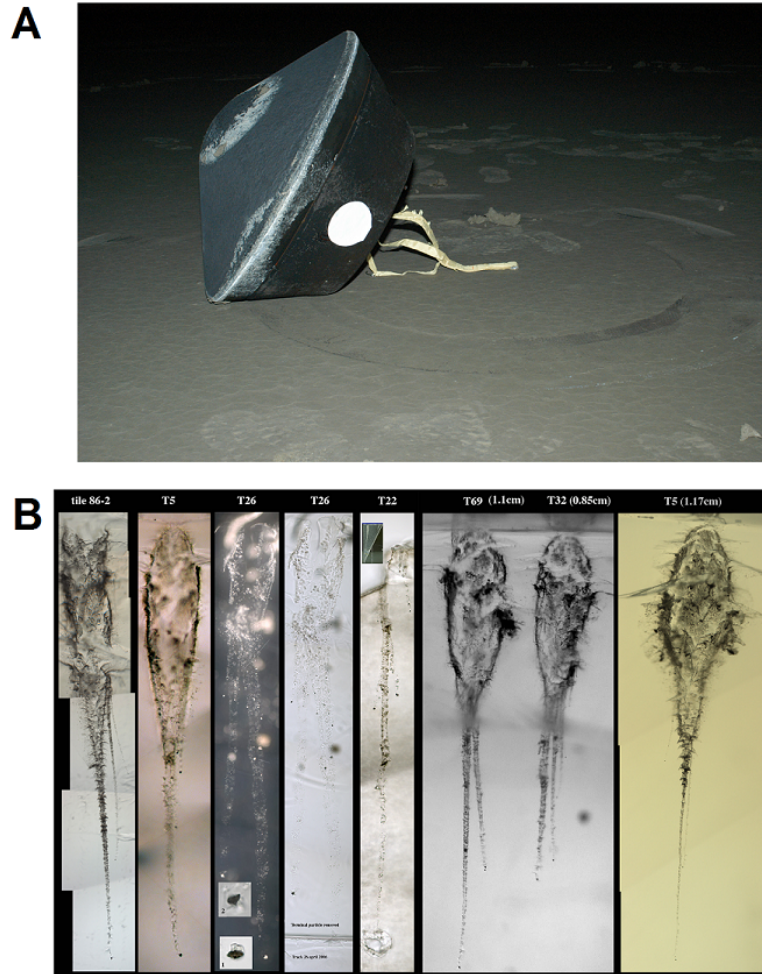


Figure 5. A) Stardust's Sample Return Capsule after landing in Utah in 2006. B) Tracks made by the impacts of comet dust within the collection tray's aerogel tiles (NASA).

2.3. Comet Dust

Comet material is thought to be some of the least altered remnants of the formation of the Solar System and have been a focus of research since first studied in situ. In 1986, several thousand comet dust particles were sampled by Vega 1, Vega 2 and Giotto in their flybys of 1P/Halley. These first cometary dust particles encountered had masses ranging from 10^{-16} to 10^{-11} g (Kissel et al, 1986). Three main types of comet dust have been identified from these initial investigations based on their chemical composition. The first group consists of rock-forming elements such as Mg, Si, Ca and Fe. A second group is composed chiefly of lighter elements H, C, N and O, dubbed the "CHON" particles. The third main group consists of particles with a mixture of both the "rock" and CHON elements. This mixed group constitutes a large portion of

all dust grains observed around comets. Approximately 50% of grain samples have significant mixtures of CHON and "rock" elements, though all grains contain some mixed composition of even the smallest degree (Fomenkova et al., 1992).

Of the "rock" type dust particles, around 50% are Mg-rich (Jessberger, 1999), and only ~10% are Fe metals, Fe sulfides or Fe oxides (Schulze et al., 1997). Silicate "rock" dust particles make up 30% of the total mass of all dust particles as measured using spectroscopy of the regions surrounding comets. Other results of spectroscopy reveal that cometary silicates range from amorphous to crystalline and roughly 80% are Mg-rich pyroxene with the remainder being mainly Mg-rich olivine (forsterite) (Harker et al., 2002).

The Stardust sample return capsule provided further insight into the composition and mineralogy of cometary dust particles. A wide range of silicate mineral grain sizes were observed. Chief among these were polycrystalline olivine grains with high Mg content and pyroxene of varied composition. These mafic silicates had densities ranging from 3-4 g cm⁻³ and diameters greater than, or equal to, 10 μm. Porous, low-density "fluffy aggregates" were observed in the samples returned by Stardust. These fluffy aggregate particles ranged greatly in size from 10⁻³ to 10² μm, had densities ~1.0 g cm⁻³, and were composed of a mixture of mafic silicates and alkali-rich sulfides (Kearsley, 2008). The majority of grains observed had these complex aggregate structures and were sub-micrometre in diameter. Nitrogen and oxygen rich organics were also observed, attributed to the CHON population of comet dust (Burchell, Kearsley 2008).

As Stardust made its close approach of 81P/Wild 2, the DFMI observed spikes in dust impact readings on time scales < 100 ms, the sensor's finest temporal resolution. This suggests that the spacecraft was crossing clouds of dust from the comet's nucleus that had been lofted by gaseous jets (Sekania et al., 2004). Though no measurements of dust distribution on a sub-kilometer scale had been made by previous comet encounters due to flyby speed or sensor capability, the two Vega spacecraft detected similarly spaced "clusters" of particles 10⁵ km from the nucleus of 1P/Halley (Simpson et al. 1987). Other spacecraft lacked the spatial resolution to discover any such distribution clusters, even if they had been present. When data from the Stardust mission is re-binned into lower resolution bins similar to these previous comet exploration missions, the dust distribution profile closely resembles these older data, and the detailed "swarms" are hidden (Tuzzolino et al., 2004).

Data from Stardust's PVDF sensors show extreme flux variation on times scales of ~100 ms, the limit of the instrument's measurements, which would suggest encounters with narrow gaseous jet plumes containing dust. However, gas flows which would contain dust particles are not always radial from their source of emission on the comet's nucleus surface. These emission features are rarely confined to narrow bands originating from a well defined active region on the nucleus surface, and more often spread conically or in fans, a function of nucleus topography and composition at their emission source.

Dust that has been freshly lofted within a jet would follow a constrained path, but as the particles traverse the coma, they become subjected to forces from gas drag. This dust spreads along gas flow boundaries between plumes originating from different locations on the nucleus (Green et al., 2004). These forces at distances greater than several nucleus radii from the comet would disrupt any ordered distribution along jet emission cones. Another local process could be at play creating these "swarms" of dust that Stardust observed well above the altitude of fresh jet emission cones. These swarms observed by Stardust are characterized by volume densities of up to 50 m^{-3} in sharp contrast with adjacent regions with a maximum 0.4 m^{-3} volume density (Green et al., 2004).

Craters within the foil of the sample collection tray were shown to have statistically significant clustering, suggesting that sets of particles with near parallel trajectories and adjacent to one another impacted at nearly the same time. Tracks within the aerogel tiles show that only ~20% of particles captured exhibited this clustering. Many of those in clusters had high incidence angles to the normal as they impacted the aerogel. Extrapolating these trajectories within the context of the spacecraft's geometry, many were found to be coming from the Whipple shield on the front of Stardust's bus. It has been postulated that impacts upon the Whipple shield should fragment dust particles that were then collected by the sample tray, though other processes might also create these tighter clusters observed in collected samples (Westphal et al., 2008).

Particle fragmentation is an expected process in the coma, and this can explain the variability in particle fluxes at scales under a kilometer, with approximately a third of particles encountered by the DFMI existing within a cluster. Confined within single 100 ms measurement intervals, or over two intervals with preceding and following measurements one to three orders of magnitude less, these extremely tight clusters could actually consist of multiple sub-clusters

that passed by the spacecraft within <100 ms and therefore were only registered as a single cluster. Therefore, greater than a third of the particles observed could belong to a much smaller cluster (Tuzzolino et al., 2004).

Additionally, particles detected together in swarms would likely be of similar mass because particle velocity is controlled by gas drag within the inner coma, a function of particle size. Particles within the coma of 81P/Wild 2 contained regions of particles of various masses, rather than homogenous grain sizes, suggesting the presence of both parent and daughter particles resulting from fragmentation (Green et al., 2004).

As particles composed of dust and volatiles are warmed by solar energy, the ices that bind these aggregates together sublime and the particles fragment into even smaller parts. If the process of local particle fragmentation is to explain these swarms, the process must either occur with low energy, imparting a very small acceleration upon daughter particles, or occur close to the spacecraft, being sampled by the DFMI before the daughter particles have had enough time to spread significantly (Green et al., 2004).

Sublimation of the volatiles that bind porous aggregate dust particles together would produce daughter fragments traveling at low velocities relative to the parent particle, unless sublimating volatiles were allowed to build up pressure within secluded pores before violently ejecting fragments. In addition to gas pressure buildup within dust pores, centrifugal forces can cause aggregate fragmentation with low separation velocities of mm s^{-1} (Westphal et al., 2008).

Another process leading to particle fragmentation would arise from charge built up on dust grains. The separation speed of a charged fragment from a charged parent particle is a function of their masses and relative charges. This process could accelerate daughter particles to velocities on the order of cm s^{-1} relative to their parent particles. If this process were responsible for fragmentation of the clustered particles collected by Stardust, fragmentation would have occurred only ~ 10 s before collection (Westphal et al., 2008).

2.4. Possibility of Companion Object

Curiously, 620 seconds after Stardust's close approach with 81P/Wild 2, approaching a distance of 4000 km from the nucleus, a spike in dust impacts was recorded. The majority, approximately 80%, of all dust impacts recorded by the DFMI at 81P/Wild 2 occurred in this region, between +620 and +720 seconds after Stardust's close encounter. These observed narrow

swarms subtended an angle of $< \sim 0.5$ degrees from the nucleus, and had particle volume densities greater than 2.0 m^{-3} contrasted with the surrounding environment's volume densities of less than 0.01 m^{-3} . For swarms like these to exist beyond 4000 km from the comet nucleus, the dust from a jet-remnant would have had to travel along near-parallel paths and with uniform velocity for days, or weeks, from a common emission source on the comet's nucleus. However this is an unlikely explanation for the existence of these observed particle swarms because of the tightly constrained dust trajectories required. More likely explanations involve dust emissions from a companion object, local secondary particle fragmentation by thermal or electrostatic forces or even forces of interparticle attraction (Green et al., 2004).

The location of this anomalous cloud of dust was between the orbital path of 81P/Wild 2, recently traversed by the comet, and its antisolar direction. This region has been thought to host companion objects of “split comets” that become fragmented, shedding pieces up to tens of meters in diameter, or in extreme cases, disintegration of the entire parent comet into numerous fragments. This kind of dramatic fragmentation was observed with comet D/1993 F2, Shoemaker–Levy 9, before the fragments collided with Jupiter in 1994. A hypothetical companion object with 81P/Wild 2 would not be gravitationally bound to the parent comet nucleus, but rather recede slowly as it established its own heliocentric orbit slightly different than that of its parent. A companion object would exhibit limited gas emission activity due to the lack of large volatile reservoirs, ejecting only smaller mass dust particles within its smaller gas production rate. This coincides with the small mass dust particles observed by Stardust within this region 4000 km from the nucleus of 81P/Wild 2, suggesting that the spacecraft may have encountered a companion object that had fragmented from the comet (Sekania et al., 2004).

2.5. Comet Plasma Environment

Solar wind interaction with comets differs from the interactions that occur with a much larger body, such as planet, possessing an enveloping magnetic field. Without the protective magnetic field, a comet's surface and enveloping coma are bombarded by high energy solar wind particles. The neutral gasses within the coma can become ionized by either photoionization from sunlight or through charge exchange with high energy Solar wind particles (Coates, Jones, 2009). This produces a source of plasma around the comet's nucleus. The production rate of gasses from

the solid volatiles within the comet's nucleus and the rate of ionization of neutral gases depend largely on the comet's heliocentric distance and the Sun's energy output (Coates, Jones, 2009).

JFCs generally have lower gas production rates, up to $\sim 10^{28}$ molecules s^{-1} , than long period comets, on the order of $\sim 10^{30}$ s^{-1} , due to their lower volatile content. Regularly traversing the inner solar system and closer to the Sun with their shorter orbital periods, JFCs more frequently are depleted of a portion of their volatile content than longer period comets that orbit much further from the Sun. The volatiles that JFCs do contain will sublime and drift away at speeds on the order of ~ 1 km/s, exceeding the $< \sim 1$ m/s escape velocity for kilometer-sized comets. These outward expanding gasses, when encountering the solar wind, can still produce bow shock features around JFCs as are seen around longer period comets. The resulting bow shock features are comparable in size to the magnetospheres of Uranus and Neptune, and the resulting plasma tails can extend several AU away from the comet nucleus (Coates, Jones, 2009).



Figure 6. In this image of comet C/2014 Q2 Lovejoy, taken from Earth, the gas and plasma tail can be seen receding away from the nucleus in the anti-Solar direction. Closer to the comet's nucleus, the coma of gas and dust spectacularly reflects sunlight (Rolando Ligustri, CARA Project, 2015).

Dusty plasmas, also referred to as complex plasmas, are composed of solid particles suspended within a plasma medium. Properties and dynamics of dusty plasma systems have been studied as phenomena of both natural environments and industrial settings. In the context of the space sciences, Dusty plasmas could exist in diverse settings ranging from planetary ionospheres and rings to cometary environments and interstellar clouds. Each of these settings could provide a natural laboratory for the in-situ research of dusty plasmas. Among these sites of naturally

occurring dusty plasma, the cometary environment has been studied and modeled extensively (Thomas et al., 1994).

Dust particles can become charged within the plasma environment of a comet's coma. Primarily, dust will pick up a negative charge through the absorption of fast electrons from the surrounding ionized gasses. Other processes can contribute to dust charging, though to a lesser extent, such as ion flow or Solar UV radiation causing photo-ejection of electrons. The rate of acquisition of charge due to electron flux within a plasma increases with increasing particle surface area (Westphal et al, 2007).

As dust particles within a plasma become charged due to electron flux, they will behave as “giant ions” and influence the surrounding plasma with their newfound electric charge. In a dusty plasma with sufficiently high number density of charged dust particles, a threshold can be crossed leading into a system that is well structured and self-ordering (Vasut et al., 2003). These self ordered systems of charged dust within a plasma occur when the electrostatic forces between charged dust particles surpass their kinetic energies. These systems are often colloquially called “plasma crystals” due to the resulting structure's resemblance to a mineral crystalline lattice, albeit at a macroscopic scale. The more precisely descriptive name of “Coulomb lattice” hints at the actual physical processes at play in the dusty plasma system (Thomas et al., 1994).

As charged dust within a plasma moves towards a more ordered arrangement, towards a lattice-like structure, the ordering can be numerically described with a Coulomb coupling parameter. This dimensionless parameter is the ratio of an average dust particle's interparticle potential energy, derived from its acquired charge from regional electron flux, to its kinetic, thermal energy. As the electrostatic potential between particles increases, overcoming the particles' individual kinetic energies, the coupling between dust particles increases and the overall system order increases (Thomas et al., 1994).

At low values of the Coulomb coupling parameter, less than 1, there is no Coulomb lattice formation, but as the parameter increases above 1, the system is said to have become strongly coupled with short range ordering. This state is also referred to as a “Coulomb liquid” where the coupling strength between charged dust particles resembles the molecular structure of a liquid. At values greater than 170, the dusty plasma exhibits long range ordering and is termed a “Coulomb solid,” resembling a molecular solid crystalline lattice (Thomas et al., 1994).

3. Methods

3.1. Observed Dust Distribution

As Stardust made its way through the inner coma region of 81P/Wild 2, the Dust Flux Monitor Instrument (DFMI) counted the dust particles encountered by its array of sensors. Each data point logged, recorded in a period of 100 ms, provides a linear profile representative of the diffuse clouds of dust that the spacecraft passed through in that time interval. In the analysis of the dust distribution surrounding 81P/Wild 2, these observed spatial clusters of dust particles have been referred to as “swarms” when observed on timescales ~ 1 s, corresponding to sampled distances of ~ 1 km, and as “bursts” on scales < 1 s and often at the limit of the DFMI's resolution, at its sample rate of 100 ms, corresponding to distances of ~ 600 m (Green et al., 2004).

The volume of each sampled burst can be derived from the surface area of the circular DFMI PVDF (polyvinylidene fluoride) thin film sensor – either the larger 200 cm² or smaller 20 cm² sensor – multiplied by the distance traveled in the sample time period (100 ms). Stardust maintained a constant velocity relative to 81P/Wild 2 for the duration of the close encounter, just over 6 km s^{-1} , so that the distance traversed within each 100 ms sampling period was about 600 m. This gives a narrow cylindrical volume that Stardust was passing through at that time, either 12 m^3 or 1.2 m^3 for the two PVDF sensor films.

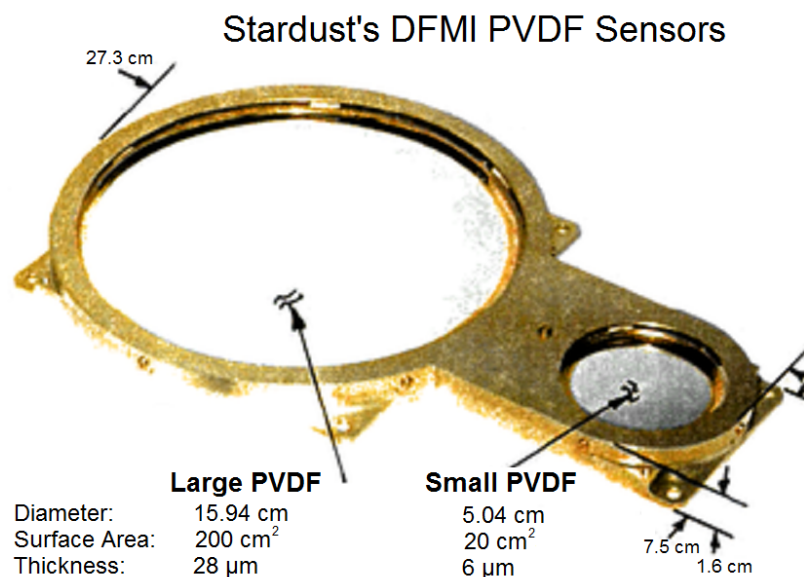


Figure 7. Image and dimensions of Stardust's DFMI PVDF sensors. The two circular sensors sampled cylindrical shaped volumes during each 100 ms sample period. The two sensors' differing assembly and film thicknesses allowed for different sized dust particles to be detected when impacting (Adapted from Tuzzolino et al., 2003).

The total number of particles encountered in this cylindrical volume provides a volume density of n particles per cubic meter. To calculate the average interparticle distance within each observed swarm or burst of dust particles, an approximation is used which assumes maximum separation distance for all particles within the volume sampled. Interparticle separation distance plays a strong role in the manifestation of coulomb lattice effects upon dust grains. Calculating the separation distance in this way assumes a homogeneous distribution within each cloud sampled and gives a minimum value for dust number density, rather than expressing heterogeneities within the sampled volume. Dust distribution heterogeneities within each volume sampled could cause the interparticle distance to vary widely above and below this average value. The average interparticle distance, assuming maximum particle separation within the sampled volume, is given by the Winger-Seitz radius equation:

$$d = (3/(4*\pi*n))^{1/3}.$$

Insight into the fine spatial resolution structures that can be present in dusty plasmas was prohibited by the limitation of the DFMI's sampling rate. Laboratory dusty plasmas, in which coulomb coupling processes have been studied, have been on scales of less than 2 cm (Thomas, 1994). Because these fine resolutions are not available within Stardust's DFMI data, particle volume density must be inferred from the total number of particles sampled within each sample period of 100 ms as calculated above with the Winger-Seitz radius.

The DFMI data used in analysis of the dusty plasma environment were limited to all instances of volumes sampled with a relatively significant dust number density. These selected data-points all had dust volume densities at the upper range of volume densities calculated for all DFMI data during the close encounter with 81P/Wild 2. This limitation on the dataset was made to target regions to be investigated for Coulomb coupling effects. Regions of higher dust number density are more likely to exhibit Coulomb coupling effects, therefore the threshold was set at a threshold of dust particle number densities greater than $10 \text{ particles m}^{-3}$.

The DFMI PVDF sensor could only sample particles with mass greater than $9.8*10^{-12} \text{ g}$. With dust particle densities at a lower limit of $\sim 1 \text{ g cm}^{-3}$ for fluffy aggregates of sub- μm mixed CHON and "rock" grains, the sensor's lower mass limit translates to a minimum detectable dust

particle size of 2.7 μm (Tuzzolino et al, 2003). Smaller particles that would not have been detected by this instrument constitute a significant portion of the dust population having fragmented from larger aggregate particles, or lofted more readily by gaseous jets from the comet's nucleus, as observed in the samples returned by Stardust (Kearsley, 2008). These smaller mass, high surface area, particles would also contribute to Coulomb lattice formation by being more readily dominated by electrostatic forces rather than kinetic. Because of these limitations of the DFMI PVDF sensors, the dust number densities calculated from observed dust data represent the lower limits of the actual particle count within the inner coma of 81P/Wild 2.

A temperature for these dust particles is determined assuming they emit only blackbody radiation. Dust temperature is given by the equation below where T_{Sol} , R_{Sol} , and D are the effective temperature, radius and distance to the sun.

$$T_d = T_{\text{Sol}} * ((R_{\text{Sol}} * (1-a))^{0.5} / (2 * D))^{0.5}$$

Dust particle albedo, a , is assumed to be 0.05 (Hadamcik, 2009), though a range of albedos for these small dust particles has only a small effect on their temperature. Holding heliocentric distance (D) constant, dust albedo change of an order of magnitude from 0.01 to 0.1 results in a temperature change of only -5 K. This provides an upper limit for particle temperature, though their actual temperature may be lower, depending on actual albedos or other thermal processes. In order to exhibit coulomb lattice behavior, the electrostatic energies of dust particles must overcome their thermal energies, therefore using a maximum value for dust temperature in calculations will require significant electrostatic forces to overcome the modeled kinetic forces.

3.2. Modeled Gas Environment

Volatile ices on the comet's surface and shallow subsurface are heated by solar insolation and sublimate, forming jets and fans of gasses extending from the solid nucleus into the surrounding space (Farnham, 2009). The products of this outgassing form the enveloping coma that surrounds the comet nucleus. Water ice is a dominant volatile in the composition of comets, including 81P/Wild 2 (de Val-Borro, 2010). This sublimation process can be modeled to provide a mass production rate per unit area, derived from observations of the active jets on the comet's surface and spectroscopy of the coma.

At the time of Stardust's flyby with 81P/Wild 2, the comet was observed to have had about 20 narrow conical jets of sublimating ices extending from its surface (Sekanina, 2004) . To visualize these active regions of the comet, the locations of the jets were plotted on top of a 81P/Wild 2 shape model using the statistical programming language R (Ihaka and Gentleman, 1996) and the rgl OpenGL 3D visualization library (Alder and Murdoch, 2015). The jet coordinates were converted from their original triaxial ellipsoidal reference frame longitude and latitude coordinates into Cartesian coordinates for plotting alongside the shape model^[1] (Ligas, 2011).

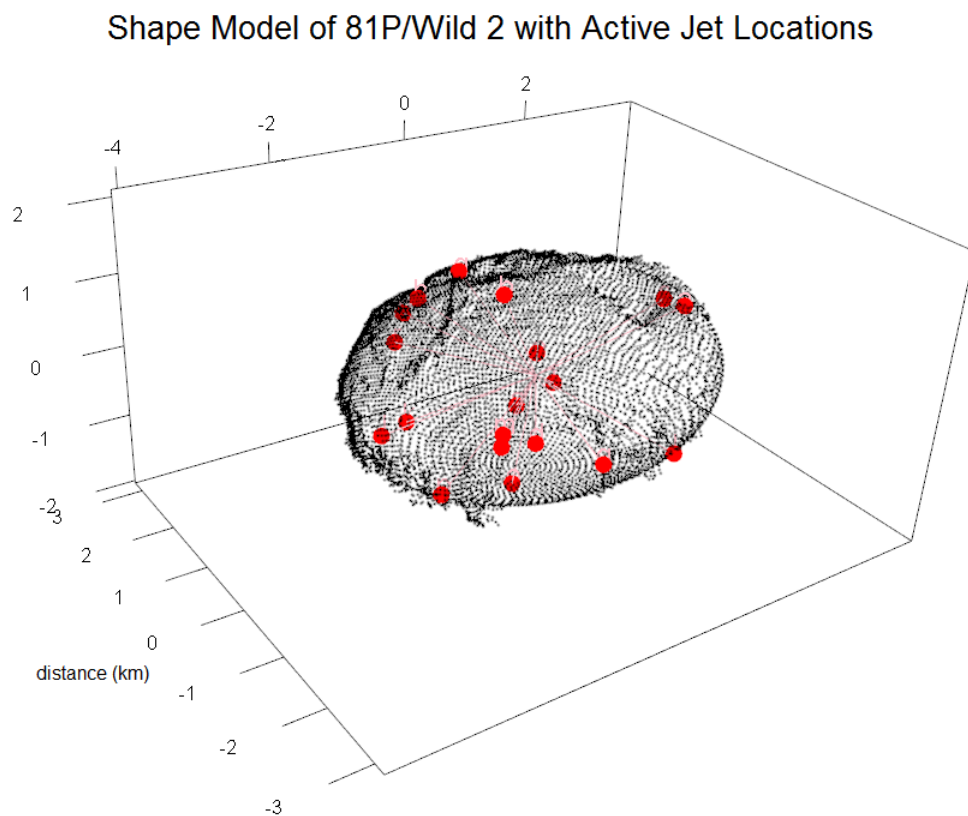


Figure 8. A shape model of 81P/Wild 2 (Ligas, 2011) plotted as a point cloud representing the comet's surface. The twenty active jet areas as identified by imagery from Stardust's flyby are marked by the red dots (Sekanina, 2004).

The water vapor production rate of 81P/Wild 2 was modeled using the active surface area as determined by Sekanina et al. Within these zones of active vapor production visualized above, the sublimation rate of a planar ice surface was used to provide a mass flow rate off of the comet nucleus surface. This was determined using the flat surface vapor pressure as derived from

investigations of water sublimation on airless bodies in space (Andreas, 2007). These calculations assume that the active areas from which jets emanate are 200 m in diameter, and within the time period Stardust observed the dust environment, sublimate water at a constant rate from a homogenous source on the nucleus surface. At a heliocentric distance of 1.9 AU the molecular water production rate of 81P/Wild is calculated to be $4.2 \cdot 10^{27} \text{ s}^{-1}$.

This value closely agrees with other investigations of water production rates of comets. Spectroscopic measurements from the Herschel Space Observatory's Heterodyne Instrument for the Far Infrared (HIFI) measured a maximum water production rate of $1.1 \cdot 10^{28} \text{ molecules s}^{-1}$ in February 2010 when 81P/Wild 2 was at a heliocentric distance of 1.61 AU (de Val-Borro, et al., 2010). Another value for 81P/Wild 2 is given as $2.0 \cdot 10^{28} \text{ molecules s}^{-1}$ near perihelion at ~ 1.6 AU (Brownlee, et al., 2004). A weakly outgassing comet model provides a lower limit to the gas production rate of $1 \cdot 10^{25} - 5 \cdot 10^{26} \text{ molecules s}^{-1}$ (Bogdanov et al. 1996). These other reported values constrain maximum and minimum production rates of water for the comet's most active period around perihelion and agree well with the value determined using the assumptions of flat surface vapor pressure, and the observed twenty active regions.

Model of Sublimation for 81P/Wild 2 and other selected comets

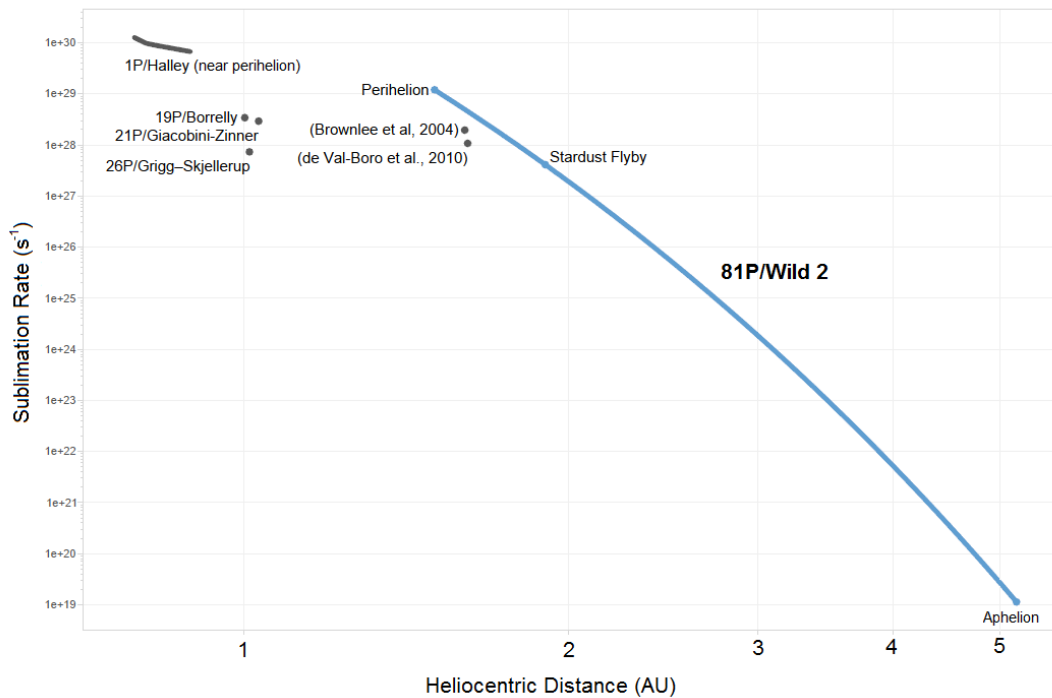


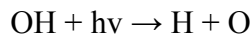
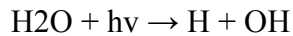
Figure 9. The model of sublimation for 81P/Wild 2 around its orbital path is presented here, from its aphelion at 5.2 AU to perihelion at 1.5 AU. Near-perihelion sublimation rates for 1P/Halley, 19P/Borrelly, 21P/Giacobini-Zinner and 26P/Grigg-Skjellerup are shown for comparison (Cravens, 2004). Values calculated from other comet sublimation models are plotted as well (Brownlee et al., 2004), (de Val-Boro et al., 2010).

3.3. Modeled Plasma Environment

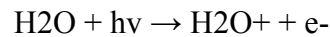
Gas products resulting from sublimation can subsequently become ionized by several processes, chiefly photoionization from solar photons (Coates, 1997). Ions and neutral gas within the inner coma expand outward from their origin at the nucleus (Edberg et al., 2015) at speeds approaching $\sim 1 \text{ km s}^{-1}$ radially away from active jet-producing areas on the nucleus until perturbed by the incoming solar wind particles which will drag tails of dust and ions away from the nucleus in the antisolar direction. For the evaluation of model the plasma around a Jupiter-Family comet such as 81P/Wild 2, the volatiles that sublimated to form the gaseous coma are assumed to be primarily water ice. A portion of the resulting water vapor within the coma is ionized via photoionization to produce the plasma environment in which dust particles reside.

To model the distribution of sublimation products around a comet nucleus, within the inner coma, Festou's vectorial model was applied (Festou, 1981). This model builds upon the Haser model of simple spherical expansion from the nucleus. Within distances of less than 10^5 km from the nucleus, the Haser model (Haser, 1957) is adequate to describe the quantity and distribution of gaseous molecules within a comet's coma close to the nucleus.

This model describes the volume density of parent and/or daughter molecules surrounding a comet. Whereas the parent molecules directly sublimated from the comet nucleus surface, daughter molecules are produced through photodissociation of the parent in one or more reaction steps. For water-dominated comet comas (Crovisier, 1989), H₂O undergoes photodissociation in sunlight separating into O and H atoms



or photoionization releasing free electrons by the reactions:



Where the energy of an incoming photon is $E = h\nu$, Planck's Constant is $h = 6.626 \times 10^{-34} \text{ Js}$, the speed of light is $c = 2.99 \times 10^8 \text{ m/s}$ and wavelength λ , and the frequency of the incoming photon is given by $\nu = c/\lambda$. Sunlight from the extreme ultraviolet and ultraviolet spectrum, with its shorter wavelengths (0.01 μm - 0.4 μm), imparts the most energy into these photodissociation reactions

(from ~3 eV to ~124 eV). The average bond dissociation energies of O-H bonds in the above reactions is about 467 kJ/mol, or 4.77 eV per bond, well within the capabilities of solar ultraviolet light. The light responsible for the majority of water photodissociation has wavelengths of $136 < \lambda < 186$ nm within the ultraviolet range (Crovisier, 1989).

The Haser model assumes a spherically symmetric point source, the comet nucleus, of outflowing parent molecules with uniform velocity (Bhardwaj, 2003). This allows the volume density of parent molecules, n_p , at a radial distance, r , from the nucleus to be calculated. The overall gas production rate at the point source nucleus is Q , and the initial gas velocity is v .

$$n_p(r) = Q / (4 * \pi * r^2 * v)$$

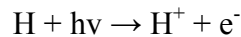
When destruction of parent molecules into daughter molecules is taken into account, with λ_p being the decay rate of the parent due to photodissociation:

$$n_p(r) = (Q / (4 * \pi * r^2 * v)) * (\exp(-rv) / \lambda_p)$$

The ion density of this plasma will be a fraction of the gas density in the coma, dependent on the distance from its point of origin. Expanding radially outward, the gas density drops as a function of r^{-2} moving away from the comet nucleus (Edberg, et al., 2015). As a product of photoionization, this plasma will have ion and electron densities approximately equal, $n_i = n_e$ (Whipple, 1985).

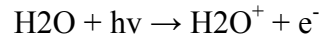
Data from the SWRI's Photo Ionization/Dissociation Rates database (Huebner and Mukherjee 2015) was used in the calculations for the photodissociation and photoionization of water and hydrogen respectively. Dependent on heliocentric distance, solar activity and the optical depth of the region surrounding the comet, photodissociation of water into H and OH ranges from $\sim 1 * 10^{-5}$ - $1.76 * 10^{-5} \text{ s}^{-1}$. Hydrogen's ionization energy of 1312 kJ/mol is only slightly less than that for Oxygen 1314 kJ/mol (~13.6 eV). The ionization energy of water is less than both Hydrogen and Oxygen at 1216 kJ/mol or ~12.6 eV.

The hydrogen gas within a comet's coma can become partially ionized through photoionization producing a plasma consisting of H^+ ions and free electrons. This occurs with a rate coefficient of $\sim 1 * 10^{-7} \text{ s}^{-1}$ producing electrons with temperatures of ~4 eV.



Water molecules, however, ionize with a greater rate coefficient of $\sim 6 * 10^{-7} \text{ s}^{-1}$ producing free electrons with temperatures of ~1 eV. Because of the lower ionization energy required to ionize water molecules over Hydrogen and Oxygen, and higher abundance of parent H_2O

molecules over daughter H and O atoms, this process is assumed to dominate the plasma composition surrounding comet 81P/Wild 2.



3.4. Coulomb Coupling

Dust suspended within the newly formed plasma will acquire a charge primarily by ion and electron collision. Because electron flow within the plasma is faster, the dust particles will pick up a net negative charge from the more influential electron collisions (Smith, et al., 2004). The charge built up on an average dust particle (in Coulombs) suspended within a plasma can be calculated (Goertz, 1989) by:

$$Q = C * S$$

where C is the dust particle's capacitance (in Farads):

$$C = (4 * \pi * \epsilon_0 * r) * \exp(-r/L_d)$$

L_d is the Debye length (m) within the plasma:

$$L_d = (k_B T_e \epsilon_0 / n_e q_e^2)^{0.5}$$

and S, the surface potential (Volts) of the dust particle is:

$$S = -2.51 * k_B * T / q_e$$

To describe the degree of ordering between charged dust particles in a dusty plasma system, the Coulomb coupling parameter quantifies the ratio of electrostatic potential energy to thermal kinetic energy of the particles (Thomas, et al., 1994). The electrostatic potential energy of a dust particle, in Joules, is given by the product of an average dust particle's charge squared and Coulomb's constant, divided by the mean interparticle distance:

$$U_e = k_e * q^2 * d^{-1}$$

The thermal energy of an average dust particle, in Joules, is quantified as the product of the average dust temperature and Boltzmann constant:

$$E_k = k_B * T$$

The ratio of these two competing energies (Joules/Joules) provides the dimensionless Coulomb coupling parameter:

$$\Gamma = U_e / E_k$$

As the electrostatic energy between particles exceeds their kinetic energies, electrostatic forces will dominate, holding charged dust particles in place relative to each other and the

surrounding plasma, leading to coupling of dust particles into a Coulomb lattice structure. These charged dust particles can act as “giant ions” (Vasut et al., 2003) as they form structure and influence the plasma that surrounds them. In a dusty plasma where the coupling parameter is greater than 1, the coupling can be described as weak. Values greater than 170 reflect systems with strong coupling, also described as “Coulomb crystals” or “Coulomb solids.”

Coulomb Coupling Parameter (Γ)	Degree of coupling
$\Gamma < 1$	no coupling
$1 < \Gamma < 170$	weak coupling (short range ordering)
$\Gamma > 170$	strong coupling (long range ordering)

4. Analysis

4.1. Stardust DFMI Observations

The data from Stardust’s DFMI as it made its close encounter with 81P/Wild 2 were evaluated to determine the location of high dust flux with respect to the comet nucleus (Green, 2004). Stardust revealed the distribution of dust with its Dust Flux Monitor Instrument ranging from the closest approach with comet 81P/Wild 2 nearly 200 km to out past 5000 km from the nucleus. The first dust particles registered by the DFMI were upon Stardust's closest approach within a window +/- 100 seconds before and after close approach, corresponding to distances within 1000 km from the nucleus. The region closest to the comet nucleus, as traversed by the spacecraft, is labeled as region A in the figure below.

Particle Spatial Distribution Spacecraft Position With Respect to 81P/Wild

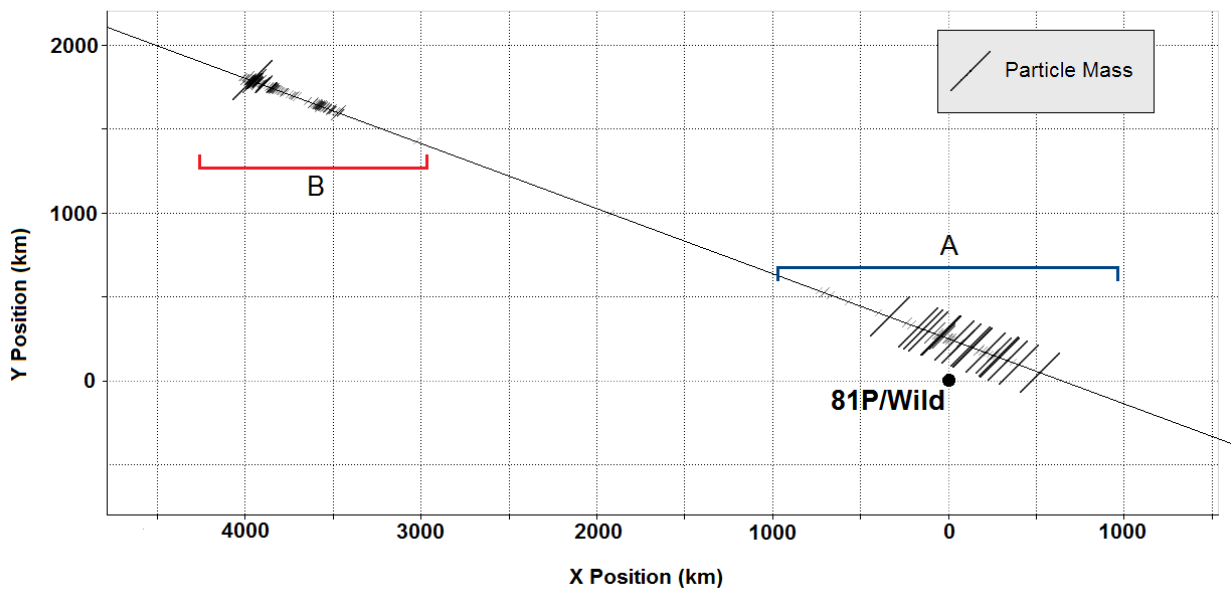


Figure 10. Relative mass of dust particles encountered by Stardust is visualized along the spacecraft's flyby path within its orbital plane reference frame (geocentric J2000).

A period of relative quiet followed this first dust cloud region, from 1000 to 3500 km past 81P/Wild 2. The second region of high dust flux encountered, region B, was between 3500 and 5000 km from the comet nucleus, 600 to 800 seconds after Stardust's close approach. Reasons for the existence of this cloud of dust at this distance from the nucleus is explored by Green and Sekania, as discussed earlier (Green, 2004; Sekania, 2004).

From the DFMI data, which provides a count of particles that fall within a specific mass threshold bin, a dust grain size was inferred assigning particles a minimum density of 1.0 g cm^{-3} assuming fluffy aggregates of CHON dust, though density could be as high as 4.0 g cm^{-3} for mafic silicate "rock" particles (Tuzzolino, 2004).

Region A had a distribution of dust grain diameters ranging from $2 \text{ }\mu\text{m}$ to greater than $150 \text{ }\mu\text{m}$ but no more than $300 \text{ }\mu\text{m}$. Of the particles encountered within this region, 94.36% had diameters between 2 and $6 \text{ }\mu\text{m}$. The dust grain sizes were even less varied within region B with 99.83% of particles encountered having diameters between 2 and $6 \text{ }\mu\text{m}$. The chart below presents a summary of the total number of particles encountered within these two regions, and the grain size distribution of each region.

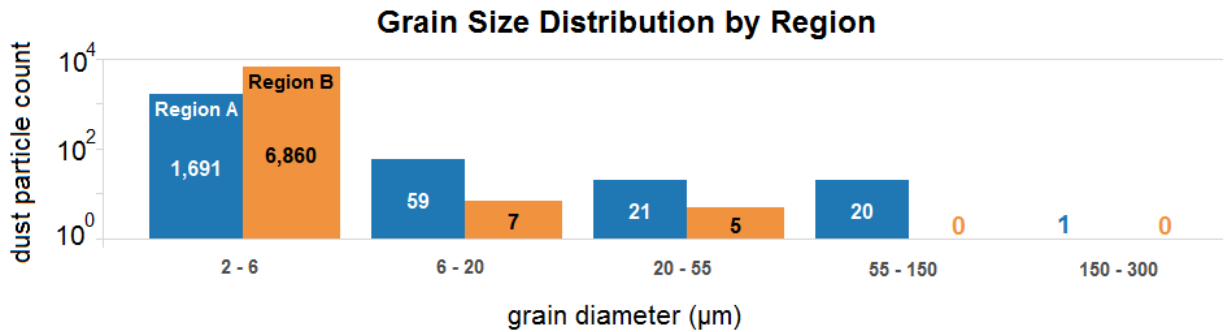


Figure 11. Grain size distribution of all dust particles encountered by Stardust’s DFMI PVDF sensors. The distribution is broken up into two regions. Region A (blue) represents the space traversed within 1000 km of the comet nucleus immediately preceding and following the spacecraft’s closest approach. Region B (orange) is the second period of greater dust particle flux, between 3500 and 5000 km from the comet nucleus.

The majority, 98.6%, of all dust impacts were detected on the DFMI channel for a mass threshold between 9.8×10^{-12} g and 1.2×10^{-10} g, suggesting that much of the comet dust population is at or below this low mass threshold. This agrees with particles collected by the Stardust Sample Return Capsule, in which sub-micron particles constituted the majority of impacts on the collection foils (Kearsley, 2008). Many of these sub-micron particles returned to Earth would not have had high enough mass to be detected by the DFMI unless they were of the denser mafic silicate “rock” population of dust.

Only in region A were significant volume densities of larger particles encountered in bursts. These particles correspond to masses between 1.2×10^{-10} and 4.3×10^{-9} g. Again assuming densities between 1 g cm^{-3} and 4 g cm^{-3} for CHON and “rock” dust grains respectively, the particle diameters detected within this mass range would be between 2 and 6 μm. No particles of mass greater than 4.3×10^{-9} contributed to the high volume density swarms and bursts observed by Stardust, although the DFMI did count some lone higher mass dust grains (Tuzzolino, 2004).

Sample points that had a dust volume density of $\geq 10 \text{ m}^{-3}$ were used for further analysis, and data points with lower dust volume densities were set aside. Because Coulomb lattice formation is highly dependent on the volume density of dust particles within a dusty plasma, only these data points were used in calculating Coulomb coupling parameters given the higher likelihood of seeing any evidence of lattice formation.

4.2. Plasma Model and Coulomb Coupling

The plasma environment encountered by Stardust was modeled in the Python programming language using Haser's model of gas expansion for the inner coma, < 10000 km from the comet nucleus^[2]. Within this region, photoionization from solar UV produces a plasma environment that is assumed to have an equal volume density of ions and electrons. Because of the low opacity of the gaseous coma, the photoionization rate due to incoming solar UV radiation does not change with distance from the comet nucleus but only with the comet's heliocentric distance. This means that the electron density of the plasma at any given point around the comet is a function of the volume density of the parent water molecules at that point.

The charging of dust particles within a dusty plasma system, is dependent on the electron density within that plasma. The electron density of this plasma of cometary origin varies with distance to the comet nucleus. The surface area of individual dust particles is heavily influential on the charge picked up while immersed within a plasma environment. Large, porous, "fluffy aggregates" of sub-micron grains spanning diameters up to several 100 um would pick up a substantial charge. With large surface areas and small masses, these aggregate particles have potential to be dominated by electrostatic forces over their kinetic energy, leading to processes such as Coulomb lattice formation. However, these larger particles were encountered infrequently by Stardust as seen in the data recorded by the DFMI, as well as the grains sampled and returned to Earth (Kearsley, 2008).

The charge imparted onto observed dust particles by electron flux within the cometary plasma can be calculated using the electron densities derived from Haser's model. Dust particles observed by Stardust would have picked up negative potentials from this electron flux of less than 9×10^{-4} V, with negative charges less than 10×10^{-19} C.

The electron densities modeled for regions within the inner coma of 81P/Wild 2 range from 1.3×10^7 to 2.3×10^8 m⁻³. The electron density of the plasma is dependent on distance from the nucleus, decreasing as the spacecraft moved away from its closest approach with 81P/Wild 2 as the inverse square of the distance from the comet.

For the plasma environment surrounding 81P/Wild 2, the degree of ionization, *a*, can be calculated as the percentage of H₂O molecules ionized out of the total population of H₂O.

$$a = n_{\text{ions}} / (n_{\text{neutrals}} + n_{\text{ions}})$$

Beginning at 100 km from the surface of the comet's nucleus, the degree of ionization is $\sim 0.002\%$. Not until a distance of ~ 600 km does the degree of ionization surpass 0.01% , a threshold for classifying weakly ionized plasmas in which common plasma behaviors begin to appear (Peratt, 1996). The degree of ionization increases beyond 0.2% at distances greater than 10000 km, beyond the scope of this model.

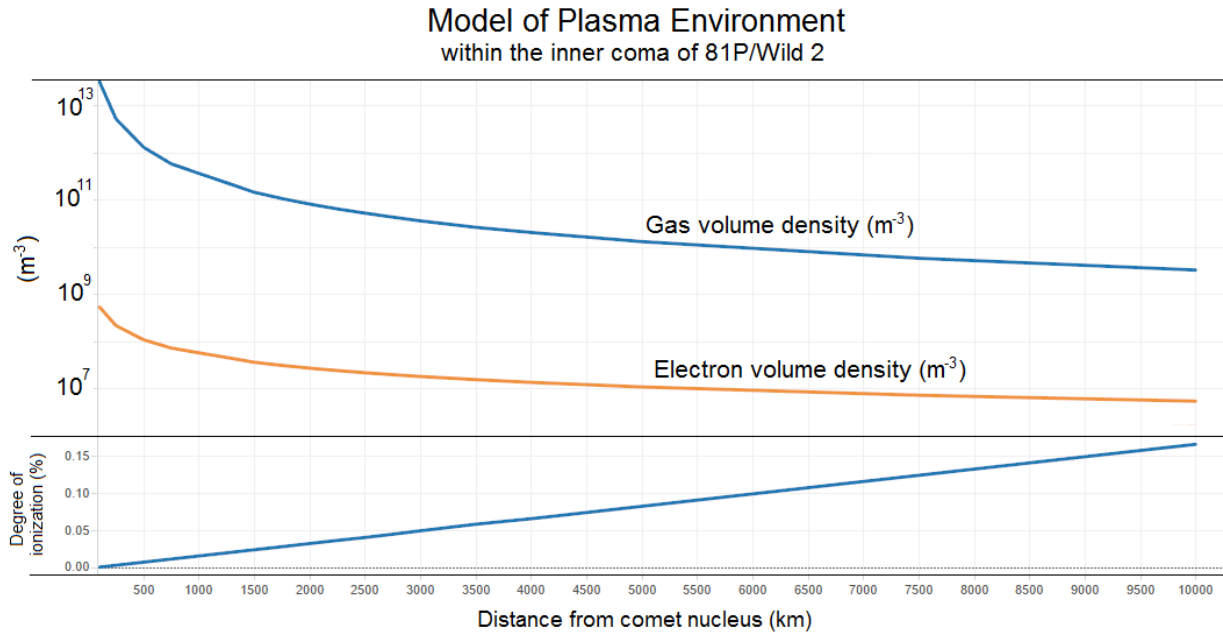


Figure 12. Electron density, and degree of ionization describe the plasma environment within the inner coma of 81P/Wild 2 at the time of Stardust's flyby, when the comet was 1.9 AU from the Sun. These are both functions of the gas volume density profile as distance from the comet nucleus increases.

The Coulomb coupling parameter for the clusters of dust particles observed by Stardust is far below the threshold for any ordering to be present in a dusty plasma system. Even for the most dense bursts sampled, where the volume density of particles is $\sim 60 m^{-3}$, a coupling parameter of only $\sim 2 \cdot 10^{-4}$ was calculated.

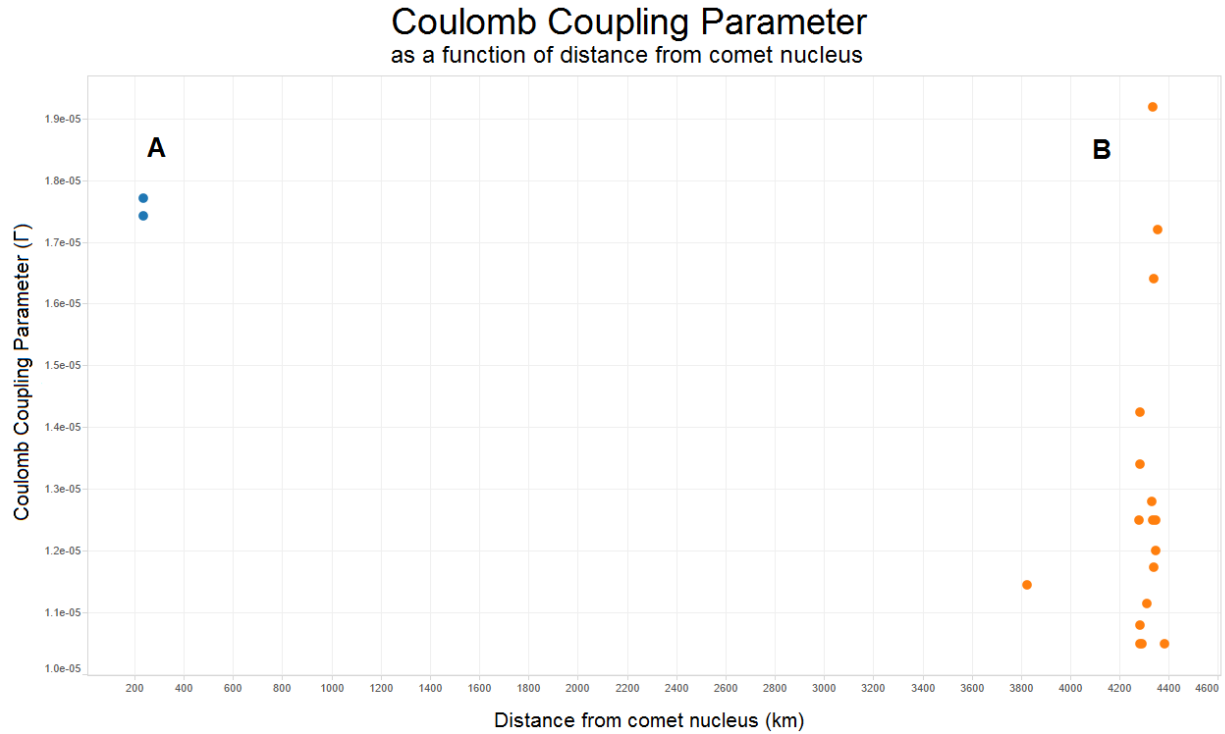


Figure 13. The calculated Coulomb Coupling Parameter values plotted, for regions A and B, against the distance from the nucleus of 81P/Wild 2. Distance from the nucleus is analogous to the electron density of the surrounding plasma environment as one recedes away from the comet. This plot shows no strong dependence on the electron density of the modeled plasma.

The Coulomb coupling parameter correlates strongly with dust particle volume density, rather than the electron density of plasma. In the model of cometary plasma developed to determine the coupling parameter, distance from the nucleus determines the density of neutral and ionized gas species and, ultimately, the electron density, which constitute the plasma environment within which the dust resides. This suggests that the modeled electron temperatures and densities of the plasma are sufficient to support coulomb lattice structures given a cloud of charged dust dense enough, though no cloud of such density was found within the area surveyed by Stardust's DFMI instrument suite.

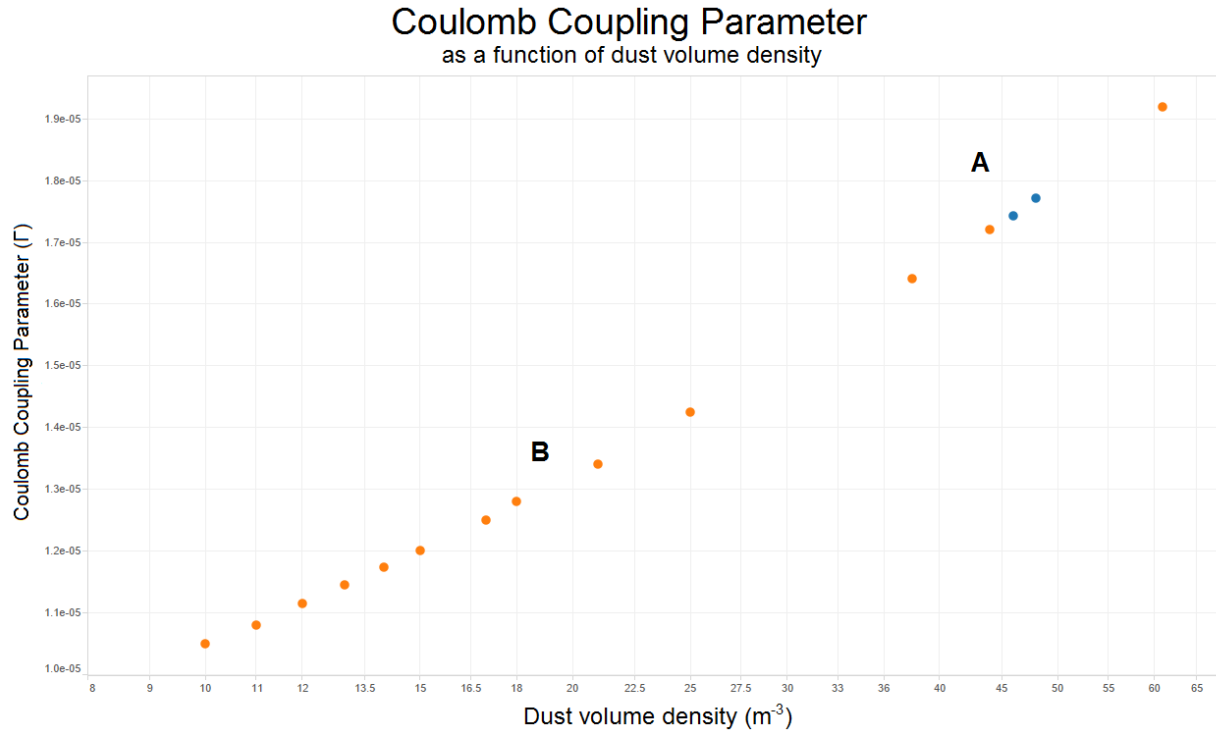


Figure 14. Within the context of this research project, the Coulomb Coupling Parameter was found to depend more strongly on the dust volume densities observed by Stardust in the vicinity of 81P/Wild 2, than with the weakly ionized plasma.

5. Discussion

5.1. Conclusions

Though no clear evidence of Coulomb lattice formation was identified, the process may still have been occurring, albeit elusively. From the model of cometary plasma at 81P/Wild 2 at the time of Stardust's flyby, it has been shown that sufficient electron density and degree of ionization are present within the near-nucleus inner coma to support the formation of Coulomb lattices. Though dust can pick up a charge from the electron flux within this plasma environment, the data collected by Stardust does not identify any region with sufficiently high dust volume density to support any strong Coulomb coupling effects. If Coulomb lattices form at all, the dynamic comet environment may prove to be too variable or violent to support such delicate structures for very long, or at scales large enough to be observed.

5.2. Limitations of Data

The DFMI sensor is heavily limited with respect to a minimum detectable particle size to perform an investigation of a process such as Coulomb lattice formation which would incorporate small particles. Based on the examination of Stardust Sample Return Capsule aerogel and foil trays, the abundance of sub-micron dust grains suggests that although these particles were not detected by the DFMI, they constitute a large portion of the dust population surrounding 81P/Wild 2.

Large aggregates of sub-micron grains, expected to have diameters on the order of 100 μm would pick up substantial charge and contribute to Coulomb lattice processes. The absence of large particles may not actually reflect the natural state of the comet's coma but rather be the result of spacecraft interference with delicate dust aggregates as discussed earlier (Westphal et al., 2007).

The sample time period and relative velocity between Stardust and 81P/Wild 2 also limited the resolution of the collected data to volumes. Because Coulomb lattices are small scale structure, often seen at scales of several centimeters in laboratory experiments (Thomas, 1994), direct observations of any such structures by Stardust wouldn't be possible. Stardust's sample rate of 100 ms^{-1} and high relative velocity with respect to 81P/Wild 2 makes its smallest spatial resolution at least an order of magnitude greater than at which Coulomb lattice structures are normally observed in the laboratory.

5.3. Future Work

After its mission to 81P/Wild 2 in 2004 and delivery of the collected samples back to Earth in 2006, Stardust embarked on a second mission to comet 9P/Tempel. This comet had been previously visited, and bombarded, by the Deep Impact spacecraft in 2005. For this new mission, Stardust-NExT, the spacecraft performed a flyby of 9P/Tempel in February of 2011, almost six years after Deep Impact's flyby, and over seven years since Stardust observed 81P/Wild 2. During the encounter with 9P/Tempel, Stardust-NExT again collected dust data with its DFMI down to a close approach distance of only 181 km. This data could be analyzed in the same manner as the data for 81P/Wild 2 to look for evidence of Coulomb lattice formation.

To gain better insight into processes within the inner coma of comets such as 81P/Wild 2, future in situ investigations could make use of suites of plasma instrumentation, and dust measurement instruments more finely tuned for a wider range of particles down to the nanometer

scale. With higher data collection rates and slower relative velocities, future spacecraft would be able to study smaller scale structures within the diffuse gas, plasma and dust of a comet's inner coma.

A mission as just described is operational at the present time. The European Space Agency's Rosetta spacecraft and Philae lander arrived in orbit around comet 67P/Churyumov–Gerasimenko in August of 2014 and have, for over a year, been studying a vast array of dynamic comet properties. Data from this mission could allow a similar investigation into the degree of Coulomb coupling close to the nucleus of this other Jupiter Family Comet.

Acknowledgements

I am very grateful for all the support and mentorship I received from many individuals while working on this project. Thank you to Dr. Susan Hoban at the University of Maryland Baltimore County (UMBC). Dr. Hoban not only supported me through her role as coordinator of NASA's Planetary Data System (PDS) Student Investigator (SI) program, but also as my mentor for this project, introducing me to the fascinating world of comets. Also thanks to my sponsoring node for the SI program, the PDS Management Node, and to the NASA PDS SI program as a whole. Thank you to the other students in our "2013+" PDS SI student cohort who shared ideas and input along the way, and to Lynne Griffith at the Center for Research and Exploration in Space Science and Technology at UMBC.

From my institution, California State Polytechnic University Pomona, I would like to thank Dr. Jascha Polet, my adviser, for her mentorship. I would also like to thank Dr. Jon Nourse, chair of Geological Sciences Department as well as the faculty and staff of the geosciences department and the Department of Physics and Astronomy at Cal Poly Pomona. And as always, I am tremendously thankful for the support of my friends and family.

Notes

1. Shape model of 81P/Wild 2 with jet locations.
Wild2Jets_Shape.R <https://github.com/SteveXe/StardustSJP>
2. Determination of Coulomb coupling parameter with Stardust data.
coulomb_coupling.py <https://github.com/SteveXe/StardustSJP>

References

- Adler, D., & Murdoch, D. (2015). RGL: 3D Visualization Using OpenGL. R package (version 0.95.1367). URL <http://cran.r-project.org/web/packages/rgl/>
- Andreas, E. (2007). New estimates for the sublimation rate for ice on the Moon. *Icarus*, 186, 24-30. doi:10.1256/qj.04.94
- Bhardwaj, A. (2003). On the Solar EUV Deposition in the Inner Comae of Comets with Large Gas Production Rates. *Geophys. Res. Lett.* Geophysical Research Letters, 30(24). doi:10.1029/2003GL018495
- Bogdanov, A., Sauer, K., Baumgärtel, K., & Srivastava, K. (1996). Plasma structures at weakly outgassing comets—results from bi-ion fluid analysis. *Planetary and Space Science*, 44(6), 519-528.
- Brownlee, D., Horz, F., Newburn, R., Zolensky, M., Duxbury, T., Sandford, S., Kissel, J. (2004). Surface of Young Jupiter Family Comet 81P/Wild 2: View from the Stardust Spacecraft. *Science*, 304, 1764-1769. doi:10.1126/science.1097899
- Burchell, M., & Kearsley, A. (2009). Short-period Jupiter family comets after Stardust. *Planetary and Space Science*, 57(10), 1146-1161. doi:10.1016/j.pss.2008.07.019
- Coates, A., & Jones, G. (2009). Plasma environment of Jupiter family comets. *Planetary and Space Science*, 57(10), 1175-1191. doi:10.1016/j.pss.2009.04.009
- Coates, A. (1997). Ionospheres and magnetospheres of comets. *Advances in Space Research*, 20, 255-255.
- Crovisier, J. (1989). The photodissociation of water in cometary atmospheres. *Astronomy and Astrophysics*, 213, 459-464.
- Economou, Thanasis E.; Green, Simon F.; Brownlee, Don E. and Clark, Ben C. (2013). Dust Flux Monitor Instrument measurements during Stardust-NExT Flyby of Comet 9P/Tempel 1. *Icarus*, 222(2) pp. 526–539.
- Edberg, N. J. T., A. I. Eriksson, E. Odelstad, P. Henri, J.-P. Lebreton, S. Gasc, M. Rubin, M. André, R. Gill, E. P. G. Johansson, F. Johansson, E. Vigren, J. E. Wahlund, C. M. Carr, E. Cupido, K.-H. Glassmeier, R. Goldstein, C. Koenders, K. Mandt, Z. Nemeth, H. Nilsson, I. Richter, G. S. Wieser, K. Szego, and M. Volwerk (2015), Spatial distribution of low-energy plasma around comet 67P/CG from Rosetta measurements. *Geophys. Res. Lett.*, 42, 4263–4269. doi: 10.1002/2015GL064233.
- Farnham, T. (2009). Coma morphology of Jupiter-family comets. *Planetary and Space Science*, 57, 1192-1217. doi:10.1016/j.pss.2009.02.008
- Farnham, T.L., T. Duxbury and J.-Y. Li, SHAPE MODELS OF COMET WILD 2, SDU-C-NAVCAM-5-WILD2-SHAPE-MODEL-V2.1, NASA Planetary Data System, 2005.
- Fomenkova, M., Kerridge, J., Marti, K., & Mcfadden, L. (1992). Compositional trends in rock-forming elements of comet Halley dust. *Science*, 258, 266-269. doi:10.1126/science.11538058
- Goertz, C. (1989). Dusty plasmas in the solar system. *Rev. Geophys. Reviews of Geophysics*, 27(2), 271-292. doi:10.1029/RG027i002p00271
- Green, S., McDonnell, A., McBride, N., Colwell, M., Tuzzolino, A., Economou, T., . . . Brownlee, D. (2004). The dust mass distribution of comet 81P/Wild 2. *J. Geophys. Res. Journal of Geophysical Research*, 109(E12S04). doi:10.1029/2004JE002318
- Green, S.F.; McBride, N.; Colwell, M.T.S.H.; McDonnell, J.A.M.; Tuzzolino, A.J.; Economou, T.E.; Clark, B.C.; Sekanina, Z.; Tsou, P. and Brownlee, D.E. (2007). Stardust Wild 2 Dust Measurements. In: Krueger, H. and Graps, A. eds. *Workshop on Dust in Planetary Systems*. ESA SP- (643). ESTEC, Noordwijk, The Netherlands: ESA Publications Division, pp. 35–44.
- Gurtler, P.; Saile, V.; Koch, E.E., Rydberg series in the absorption spectra of H₂O and D₂O in the vacuum ultraviolet, *Chem. Phys. Lett.*, 1977, 51, 386. doi:10.1088/0022-3700/11/6/012
- Hadamcik, E., & Lvasseur-Regourd, A. (2008). Optical properties of dust from Jupiter family comets. *Planetary and Space*

- Science, 57, 1118-1132. doi:10.1016/j.pss.2008.10.015
- Harker, D., Wooden, D., Woodward, C., & Lisse, C. (2002). Grain Properties of Comet C/1995 O1 (Hale-Bopp). The Astrophysical Journal, 580, 579-597. doi:10.1086/343091
- Huebner, W.F., Mukherjee, J., Photoionization and photodissociation rates in solar and blackbody radiation fields, Planetary and Space Science (2015), <http://dx.doi.org/10.1016/j.pss.2014.11.022>
- Huebner, W.F., Carpenter, C.W., Solar Photo Rate Coefficients, Los Alamos Scientific Laboratory report LA-8085-MS (1979).
- Ihaka, R. and Gentleman, R. (1996), R: A Language for Data Analysis and Graphics, Journal of Computational and Graphical Statistics, 5(3), 299–314.
- Jessberger, E., Christoforidis, A., & Kissel, J. (1988). Aspects of the major element composition of Halley's dust. Nature, 332, 691-695. doi:10.1038/332691a0
- Kearsley, A. T., Borg, J., Graham, G. A., Burchell, M. J., Cole, M. J., Leroux, H., Bridges, J. C., Hörz, F., Wozniakiewicz, P. J., Bland, P. A., Bradley, J. P., Dai, Z. R., Teslich, N., See, T., Hoppe, P., Heck, P. R., Huth, J., Stadermann, F. J., Floss, C., Marhas, K., Stephan, T. and Leitner, J. (2008), Dust from comet Wild 2: Interpreting particle size, shape, structure, and composition from impact features on the Stardust aluminum foils. Meteoritics & Planetary Science, 43: 41–73. doi: 10.1111/j.1945-5100.2008.tb00609.x
- Kissel J. et al. (1986) Composition of Comet Halley dust particles from Vega observations. Nature, 321, 280–282. doi:10.1038/321280a0
- Ligas, M. (2011). Cartesian to geodetic coordinates conversion on a triaxial ellipsoid. J Geod Journal of Geodesy, 86(4), 249-256. doi:10.1007/s00190-011-0514-7
- Marsden, B. (2008). Orbital properties of Jupiter-family comets. Planetary and Space Science, 57, 1098-1105. doi:10.1016/j.pss.2008.12.007
- Peratt, A. (1996). Advances in Numerical Modeling of Astrophysical and Space Plasmas. Plasma Physics, 242(1), 51-75. doi:10.1007/BF00645112
- Schulze, H., Kissel, J., & Jessberger, E. (1997). Chemistry and Mineralogy of Comet Halley's Dust. From Stardust to Planetesimals, 122, 397-414.
- Sekanina, Z., Brownlee, D., Economou, T., Tuzzolino, A., & Green, S. (2004). Modeling the Nucleus and Jets of Comet 81P/Wild 2 Based on the Stardust Encounter Data. Science, 1769-1774. doi:10.1126/science.1098388
- Semenov, B.V., R.L. Newburn, H.W. Taylor, C. Hash, and C.H. Acton, T.L. Farnham, STARDUST NAVCAM IMAGES OF WILD 2, SDU-C-NAVCAM-2-EDR-WILD2-V2.0, NASA Planetary Data System, 2008.f
- Semenov, B.V., A.J. Tuzzolino, J.A.M. McDonnell, H.W. Taylor, and C.H. Acton, STARDUST DFMI WILD 2 ENCOUNTER EDR DATA, SDU-C-DFMI-2-EDR-WILD2-V1.0, NASA Planetary Data System, 2004.
- Smith, B., Vasut, J., Hyde, T., Matthews, L., Reay, J., Cook, M., & Schmoke, J. (2004). Dusty plasma correlation function experiment. Advances in Space Research, 34(11), 2379-2383. doi:10.1016/j.asr.2003.07.073
- Thomas, H., Morfill, G., Demmel, V., Goree, J., Feuerbacher, B., & Möhlmann, D. (1994). Plasma Crystal: Coulomb Crystallization in a Dusty Plasma. Phys. Rev. Lett. Physical Review Letters, 73(5), 652-655. doi:10.1103/PhysRevLett.73.652
- Tuzzolino, A., et al. (2003). Dust Flux Monitor Instrument for the Stardust mission to comet Wild 2. J. Geophys. Res. Journal of Geophysical Research, 108(E10). doi:10.1029/2003JE002086
- Tuzzolino, A., et al. (2004). Dust Measurements in the Coma of Comet 81P/Wild 2 by the Dust Flux Monitor Instrument. Science, 304, 1776-1780. doi:10.1126/science.1098759
- Westphal, A., et al. (2007). Discovery of non-random spatial distribution of impacts in the Stardust cometary collector.

Meteoritics & Planetary Science, 43(1), 415-429.

Tsou, P., et al. (2004). Stardust encounters comet 81P/Wild 2. *J. Geophys. Res. Journal of Geophysical Research*, 109(E12). doi:10.1029/2004JE002317

M. de Val-Borro, P. Hartogh, J. Crovisier, D. Bockelée-Morvan, N. Biver, D. C. Lis, R. Moreno, M. Rengel, S. Szutowicz, M. Banaszkiewicz, F. Bensch, M. I. Bł ecka, M. Emprechtinger, E. Jehin, M. Küppers, L.-M. Lara, E. Lellouch, B. M. Swinyard, B. Vandenbussche, G. A. Blake, J. A. D. L. Blommaert, J. Cernicharo, L. Decin, P. Encrenaz, C. Jarchow, T. Encrenaz, E. A. Bergin, T. de Graauw, D. Hutsemékers, M. Kidger, J. Manfroid, A. S. Medvedev, D. A. Naylor, R. Schieder, N. Thomas, C. Waelkens, R. Szczerba, P. Saraceno, A. M. Di Giorgio, S. Philipp, V. Ossenkopf, P. Zaal, and R.

Shipman, D. Stam, T. Klein (2010). Water production in comet 81P/Wild 2 as determined by Herschel/HIFI. *Astronomy & Astrophysics*, 521(L50). doi:10.1051/0004-6361/201015161

Vasut, J., Hyde, T.W., & Barge, L. (2004). Finite Coulomb Crystal Formation. *Advances in Space Research*, 34(11), 2396-2401. doi:10.1016/j.asr.2003.02.071

Whipple, E. C., T. G. Northrop, and D. A. Mendis (1985), The electrostatics of a dusty plasma, *J. Geophys. Res.*, 90(A8), 7405–7413, doi:10.1029/JA090iA08p07405.